

The photometric observation of the quasi-simultaneous mutual eclipse and occultation between Europa and Ganymede on 22 August 2021

Chu Wing So^{a,*}, Godfrey Ho Ching Luk^b, Giann On Ching Chung^b, Po Kin Leung^b, Kenneth Ho Keung Hui^c, Jack Lap Chung Cheung^a, Ka Wo Chan^a, Edwin Lok Hei Yuen^d, Lawrence Wai Kwan Lee^a, Patrick Kai Ip Lau^e, Gloria Wing Shan Cheung^a, Prince Chun Lam Chan^a and Jason Chun Shing Pun^d

^aHong Kong Space Museum, 10 Salisbury Road, Tsim Sha Tsui, Kowloon, Hong Kong, China

^bDepartment of Physics, The Chinese University of Hong Kong, Sha Tin, New Territories, Hong Kong, China

^cHo Koon Nature Education cum Astronomical Centre (Sponsored by Sik Sik Yuen), 101 Route Twisk, Tsuen Wan, New Territories, Hong Kong, China

^dDepartment of Physics, The University of Hong Kong, Pok Fu Lam, Hong Kong, China

^eHong Kong Science Museum, 2 Science Museum Road, Tsim Sha Tsui East, Kowloon, Hong Kong, China

ARTICLE INFO

Keywords:

Astrometry

Eclipses

Jupiter, satellites

Occultations

Photometry

ABSTRACT

Mutual events (MEs) are eclipses and occultations among planetary natural satellites. Most of the time, eclipses and occultations occur separately. However, the same satellite pair will exhibit an eclipse and an occultation quasi-simultaneously under particular orbital configurations. This kind of rare event is termed as a quasi-simultaneous mutual event (“QSME”). During the 2021 campaign of mutual events of jovian satellites, we observed a QSME between Europa and Ganymede. The present study aims to describe and study the event in detail. We observed the QSME with a CCD camera attached to a 300-mm telescope at the Hong Kong Space Museum Sai Kung iObservatory. We obtained the combined flux of Europa and Ganymede from aperture photometry. A geometric model was developed to explain the light curve observed. Our results are compared with theoretical predictions (“O-C”). We found that our simple geometric model can explain the QSME fairly accurately, and the QSME light curve is a superposition of the light curves of an eclipse and an occultation. Notably, the observed flux drops are within 2.6% of the theoretical predictions. The size of the event central time O-C’s ranges from -14.4 to 43.2 s. Both O-C’s of flux drop and timing are comparable to other studies adopting more complicated models. Given the event rarity, model simplicity and accuracy, we encourage more observations and analysis on QSMEs to improve Solar System ephemerides.

1. Introduction

Mutual events (MEs or mutual phenomena) are eclipses and occultations among planetary satellites. For the jovian, saturnian and uranian systems, a series of MEs happen about every 6, 14 and 42 years respectively (Arlot and Emelyanov, 2019) when the Sun crosses the planetary equatorial plane (mutual eclipse) or when Earth crosses such a plane (mutual occultation). ME observations have been extended to binary asteroids (Descamps et al., 2008; Berthier et al., 2020).

Numerous observations have been made on MEs whenever the occasion arose since the 1970s (see Arlot and Emelyanov (2019) for a recent review). Much information about the satellite systems can be obtained from ME observations. For example, since the reduction of the satellites’ flux during ME depends on how sunlight is reflected or scattered from the satellites, results from ME photometric observations place constraints on the eclipsed/occulted satellite’s albedo, surface hot spots associated with volcanism (Fujii et al., 2014; Descamps et al., 1992; Goguen et al., 1988), limb darkening and atmosphere existence (Aksnes, 1974), etc.

The positions of the satellites also determine the details of flux reduction. Extracting astrometric information from the ME’s photometric data has been one of the direct ways to construct satellite ephemerides (Arlot and Emelyanov, 2019; Saquet et al., 2016; Lainey et al., 2004a). On the other hand, the comparisons between observations and theoretical computations (known as “O-C”) facilitate the improvement of existing satellite ephemerides and the theories

of satellite motion (Emelyanov, 2020; Arlot and Emelyanov, 2019; Saquet et al., 2018, 2016; Arlot et al., 2014; Emelyanov, 2003; Arlot et al., 2009; Emelyanov, 2002).

ME astrometry can now achieve an accuracy close to that of HST observations (Arlot and Emelyanov, 2019) using sensitive semiconductor sensors such as CCD cameras. By analysing highly accurate and long-term data, one can reveal the satellite’s interior structure and dynamics (Arlot and Emelyanov, 2019; Arlot et al., 2014; Emelyanov et al., 2011; Arlot et al., 2009; Vienne, 2008; Aksnes and Franklin, 2001), confirm the depth of oceans (Noyelles et al., 2004) and the planet–satellite tidal dissipation (Lainey et al., 2009).

Jupiter’s Galilean satellites (J1: Io; J2: Europa; J3: Ganymede; J4: Callisto) are the most studied dynamical systems. Their MEs have received much attention because they are relatively easier to observe and occur more frequently. In addition, due to the absence of atmosphere on Galilean satellites, the accuracy of ME astrometry can exceed the diffraction limit of a telescope (Vienne, 2008) or has a 1σ accuracy of about $0.025''$ (Lainey et al., 2009). However, almost all of the previous studies of Galilean MEs limited the scope to individual eclipses or occultations only. Indeed, if MEs occur near the time of jovian opposition, mutual eclipses and occultations may happen almost simultaneously as the shadow of the active satellite is very close to (or even overlaps with) the active satellite itself from the Earth’s perspective. Fig. 1 shows simulated examples. It is also possible that the shadow of another satellite (other than the occulting satellite) projects on the passive satellite which is being occulted (see Sect. 6). In both cases, an occultation/eclipse will start before the end of an eclipse/occultation on the passive satellite. We name this kind of special event a “quasi-simultaneous mutual event” or “QSME”. A QSME’s duration is typically longer than that of an ordinary ME (which takes several minutes to tens of minutes only (Emelyanov, 2020; Arlot and Emelyanov, 2019)) and may last for more than an hour.



Figure 1: Simulated examples of QSMEs. (a)–(c) are events with shadows overlapping with the active satellites, while (d)–(f) are events without shadows overlapping. (a) is the event in the present study. (c) is the event described in Vasundhara (1994). (b) & (d) happened in-front-of Jupiter. Different events are not drawn in the same scale. The simulations are created with WinJUPOS (<http://www.grischa-hahn.homepage.t-online.de/>).

In this paper, we adopt the standard designating practice: the code 3E2 means J3 eclipses J2; 3O2 means J3 occults J2, etc.

This study does not focus on “double eclipse” (i.e., two eclipses happen quasi-simultaneously, see Emelyanov et al. (2022) for a double eclipse example occurred on 19 April 2021) or “double occultation” (i.e., two occultations happen quasi-simultaneously). Besides, we will not discuss close pairs of separated MEs in which an eclipse/occultation happens immediately after/before an eclipse/occultation (e.g., see Aksnes and Franklin, 1976, Berthier et al., 2020). Lastly, we skip the discussion on the “simultaneous mutual event” (“SME”), which is possible in theory but is probably extremely rare as it requires a pair of ME to occur *exactly* simultaneously.

QSMEs have been under-researched. To look for a QSME, observers have to go through the prediction lists and check the time intervals of individual MEs one-by-one to see if another ME starts before the end of an ME on the passive satellite. Many other authors and observers were aware of QSMEs, but little attention was paid to detailed examination. For example, Price (2000) introduced the QSMEs on 18 February 1932 and 19 August 2003 (simulated in Fig. 1(b)).

Table 1*MULTI-SAT*'s predictions of the QSME on 22 August 2021.

	3E2	3O2
Begin time, t_{begin} (hour after 13:00)	0.984	1.565
Central time, $t_{central}$ (hour after 13:00)	1.513	2.007
End time, t_{end} (hour after 13:00)	2.044	2.448
Impact parameter, x (arcsec)	0.0245	0.4053
Flux drop ratio, ΔI	0.6530	0.6584

Some researchers skipped the analysis or left the analysis for “future works” even though several QSMEs in 2003, 2009 and 2014–15 were observed or listed (Pauwels et al., 2005). Without going into further details, other works published the QSME light curves with two minima for each when QSMEs took place on 26 January 1991 (Fig. 1(f)) (Mallama, 1992; Emelyanov and Arlot, 2020) and 3 February 2003 (Fig. 1(e)) (Arlot et al., 2009). Amateur astronomers¹ also observed the QSMEs in 2009 and 2015.

Noyelles et al. (2003) analysed a QSME between saturnian satellites Enceladus and Tethys on 14 September 1995. However, the existence of two light curve minima was doubtful as the data signal-to-noise ratio was low.

As far as we know, the only work that attempted to analyse jovian QSME was done by Vasundhara (1994). The author analysed a QSME of 2O1 then 2E1 on 29 January 1991 (simulated in Fig. 1(c)) and described it as an “overlapping” or a “composite” event. The light curve was fitted with theoretical models that help derive the relative astrometric positions of the satellites. However, we cannot repeat the analysis due to the lack of published data and sufficient details of the model (but see Sect. 5.2 where we analysed the same event from different observations using our model).

Here we present a QSME observed with a 2-megapixel CCD camera attached to the prime focus of a 300-mm reflector in Sai Kung, Hong Kong on 22 August 2021. We report that the QSME photometric light curve is a kind of combination of eclipse and occultation effects. To characterise the QSME, a new model is developed. The observed light curve is fitted with the model and an O-C analysis is conducted.

This paper is organised as follows. The details of the observations, data reduction and model are presented in Sect. 2 to Sect. 4 respectively. Sect. 5 presents the results. Finally, we draw conclusions and initiate discussions in Sect. 6.

2. Observations

The Natural Satellites Ephemeride Server *MULTI-SAT* (Emelyanov and Arlot, 2008) predicted 242 Galilean MEs globally for the PHEMU21 observation campaign in 2021 (Arlot and Emelyanov, 2020). Considering the Jupiter–Sun angular separation, only 192 events were observable from 3 March 2021 to 16 November 2021. See Emelyanov et al. (2022) for the report on the astrometric results of the campaign. QSMEs were rare: there was only one predicted occurrence (3E2 + 3O2, simulated in Fig. 1(a)) between 13:59 and 15:26 on 22 August (UTC time, same hereafter). *Occult* software² predicted an additional QSME (3O2 + 3E2, simulated in Fig. 1(d)) between 16:24 and 17:46 on 15 August. Neither events were observed in Emelyanov et al. (2022).

We observed the one on 22 August but lost the one on 15 August due to bad weather conditions. The 15 August occurrence was unfavourable for photometric observation because the satellites were in transit across Jupiter during the entire QSME. The jovian disc’s brightness overwhelmed the satellite’s light in that case.

Table 1 tabulates the *MULTI-SAT*'s predictions based on Lainey et al. (2009)'s theory for the 22 August event.

The observation was conducted at the Hong Kong Space Museum Sai Kung iObservatory (IAU observatory code: D19; telescope position: 22°24'29.3"N, 114°19'22.6"E, 92.5 m above sea level), which is located in Pak Tam within the Sai Kung West Country Park, New Territories, Hong Kong. See So and Leung (2019); So (2014) and Pun et al. (2013) for the site’s quality, i.e. light pollution conditions. We attempted to observe the event independently at the Ho Koon Nature Education cum Astronomical Centre in Tsuen Wan (about 22.3 km west of iObservatory), but it was cloudy at that location. Observing steps and procedures followed Arlot and Emelyanov (2020, 2019).

We used the Takahashi Mewlon-300 Dall–Kirkham Cassegrain telescope (primary mirror of 300 mm diameter, focal length of 2960 mm) on the Takahashi EM-500 Temma II German equatorial mount (tracked at the sidereal rate

¹<https://skyandtelescope.org/astronomy-news/mutual-event-season-heats-up-at-jupiter/>.

²<http://www.lunar-occultations.com/iota/occult4.htm>.

of $15.041'' \text{ s}^{-1}$), equipped with the Lumenera SKYnyx2-2C with a colour CCD chip at the prime focus. The chip has a matrix of 1616×1216 pixels of $4.4 \times 4.4 \mu\text{m}$. The setup corresponds to an effective field-of-view (FOV) of $8.4' \times 6.0'$. The chip's spectral responses to different colours are presented in Fig. 2. No additional filter was applied. No track guiding was adopted because the polar alignment was performed accurately. The camera does not have a cooling feature.

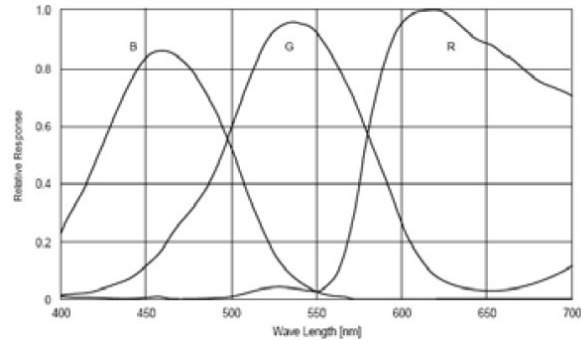


Figure 2: Spectral responses of the SKYnyx2-2C camera. Obtained from <https://www.lumenera.com/media/wysiwyg/resources/documents/datasheets/astro/skynyx2-2-datasheet.pdf>

We imaged Jupiter, J2 and J3 (both involved in the QSME) and J1 (not involved in the QSME but used as the photometric reference) within the same frame in Flexible Image Transport System (FITS) format. The images were slightly de-focused to avoid saturation while maintaining a reasonable target signal-to-noise ratio. While the telescope's optical axis was slightly misaligned, leading to the deformation of satellite images, the photometric accuracy was unaffected because the stellar aperture included all light from both satellites (see below). Continuous unbinned exposures, each at 1.5 s, were made from 13:55 (around 5 min before the QSME) to 15:56 (around 30 min after the QSME) to measure the satellites' brightness outside the QSME. A total of 3138 sequential images were analysed in this study. We used *MaxIm DL 6* software³ for image acquisition.

To get accurate timing, the laptop's clock was synchronised with a GPS antenna cum the NTP server Microsemi SyncServer S80, which received time signals directly from the Global Navigation Satellite System (GNSS) satellites. Compared with the method using online time synchronisation services, our method avoided time delay when the time signal passed through the internet. Good GNSS satellite signals with 13 satellite views were received throughout the observation. After getting the shutter latency (0.33 s, measured prior to the observations) *MaxIm DL* timestamped each image to one-hundredth of a second precision. The timestamp was considered as the mid-time of each exposure.

3. Data reduction

We performed aperture photometry separately on the J2–J3 pair and J1 on each image with *MaxIm DL 6*. While it was possible to record the light variations of the eclipsed satellite during an ordinary mutual eclipse in previous studies, the total combined flux from J2 (the eclipsed and occulted satellite) and J3 (the eclipsing and occulting satellite) rather than their individual fluxes was measured because they were indistinguishable in the image most of the time in our case. After some testing, we chose 40 pixels as the optimal aperture radius. Note that this aperture size is relatively large compared to the usual stellar photometry. This aperture is large enough to contain the light from the J2–J3 pair even 30 min after the QSME. Another reason for using a larger-than-usual aperture is that the images were de-focused and exhibited a wider point spread function, as mentioned previously. The radius of the sky annulus and its width are 50 and 10 pixels respectively. Fig. 3 shows the setting overlaid on a sample image. We also conducted photometry independently with the *phot* task under the *NOAO.DIGIPHOT.APPHOT* package in the Image Reduction and Analysis Facility (IRAF) written at the National Optical Astronomy Observatories (NOAO). Similar results were obtained.

To construct the light curve, for each image we calculated the flux ratio $E = f_{\text{event}}/f_{\text{reference}}$, where f_{event} and $f_{\text{reference}}$ are the fluxes obtained from the J2–J3 event pair and the J1 reference respectively. By dividing, atmospheric influence will be eliminated because the satellites were close to each other in the sky and experienced the (assumed) same atmospheric influence. The bias and dark corrections were incorporated in our data reduction.

³<https://diffractionlimited.com/product/maxim-dl/>.

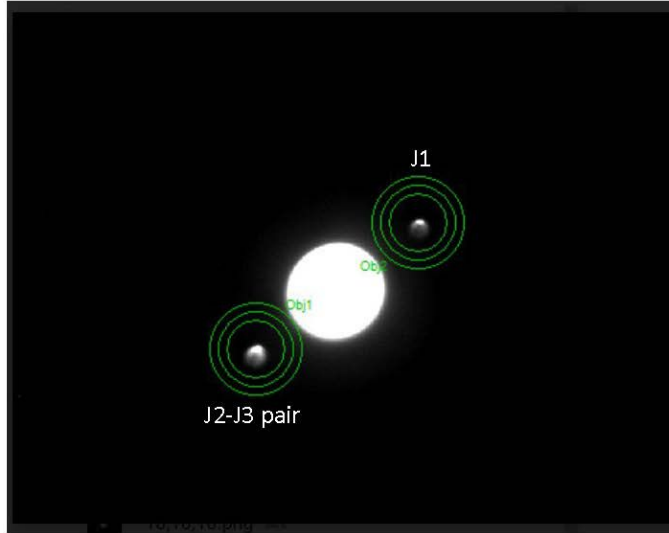


Figure 3: Setting of aperture photometry: on each target, the innermost circle shows the aperture radius; the region between the outermost and the middle circles is the sky annulus. The saturated disc at the centre is Jupiter.

Fig. 4(b) presents the light curve with very good data quality. A significant flux drop is evident. For ease of understanding, we added the event simulation, created based on Lainey et al. (2006, 2004b,a), in Fig. 4(a). When comparing the simulation with the observations, one can see that there is a gradual light drop attributed to the 3E2 near the beginning. A part of the observed drop near the middle combines an eclipse rise and an occultation drop. The combination produces the asymmetric light curve (ordinary MEs have near symmetric light curves, but see Vasundhara et al. (2017)). There is a “bump” with a small (2%–3%) brightness increase peaked at 1.86 h after 13:00 (or near 14:52). The bump is attributed to the “short-lived” period when J2 was leaving J3’s shadow and was soon partially blocked by J3 (Fig. 4(a)). Remarkably, the light curve exhibits two minima in which the second minimum (attributed to 3O2) is slightly brighter than the first one (attributed to 3E2) since the occultation was not a total occultation while the eclipse was a total eclipse. Near the end of QSME, the overall brightness returned gradually after 3O2 and levelled off.

A geometrical model can be used to describe the shape of the light curve. The model is the theme of Sect. 4.

4. QSME model

As mentioned in Sect. 1, few researchers have formulated QSME geometric models. We attempt to develop our model to obtain astrometric data from the light curve.

First, we express the measured flux E_i at the i th observation made at time t_i as (Emelyanov, 2020):

$$E_i = K \cdot S(t_i), \text{ for } i = 1, 2, \dots, n \quad (1)$$

where $S(t_i)$ is the normalised theoretical flux of the satellite(s) at time t_i , n is the total number of observations on the same event and K is the proportionality constant relating observation and theory. The key of the model is to describe S in the form of:

$$S(t_i) = \frac{p_a \pi r_o^2 + p_p \times [\pi r_p^2 - k_{ep}(t) - k_{op}(t) + k(t)]}{p_a \pi r_o^2 + p_p \pi r_p^2}. \quad (2)$$

Throughout the model, the subscript e represents the parameters related to the eclipsing satellite’s umbra, the subscript o represents the parameters related to the occulting satellite, the subscripts a and p represent the parameters related to the active (eclipsing and/or occulting) and passive (eclipsed and/or occulted) satellites respectively.

In Eq. 2, p ’s and r ’s are the albedos and the apparent radii respectively. They are constants throughout the event. Here, instead of considering a complicated model that involves umbra and penumbra, as well as the gradual decrease

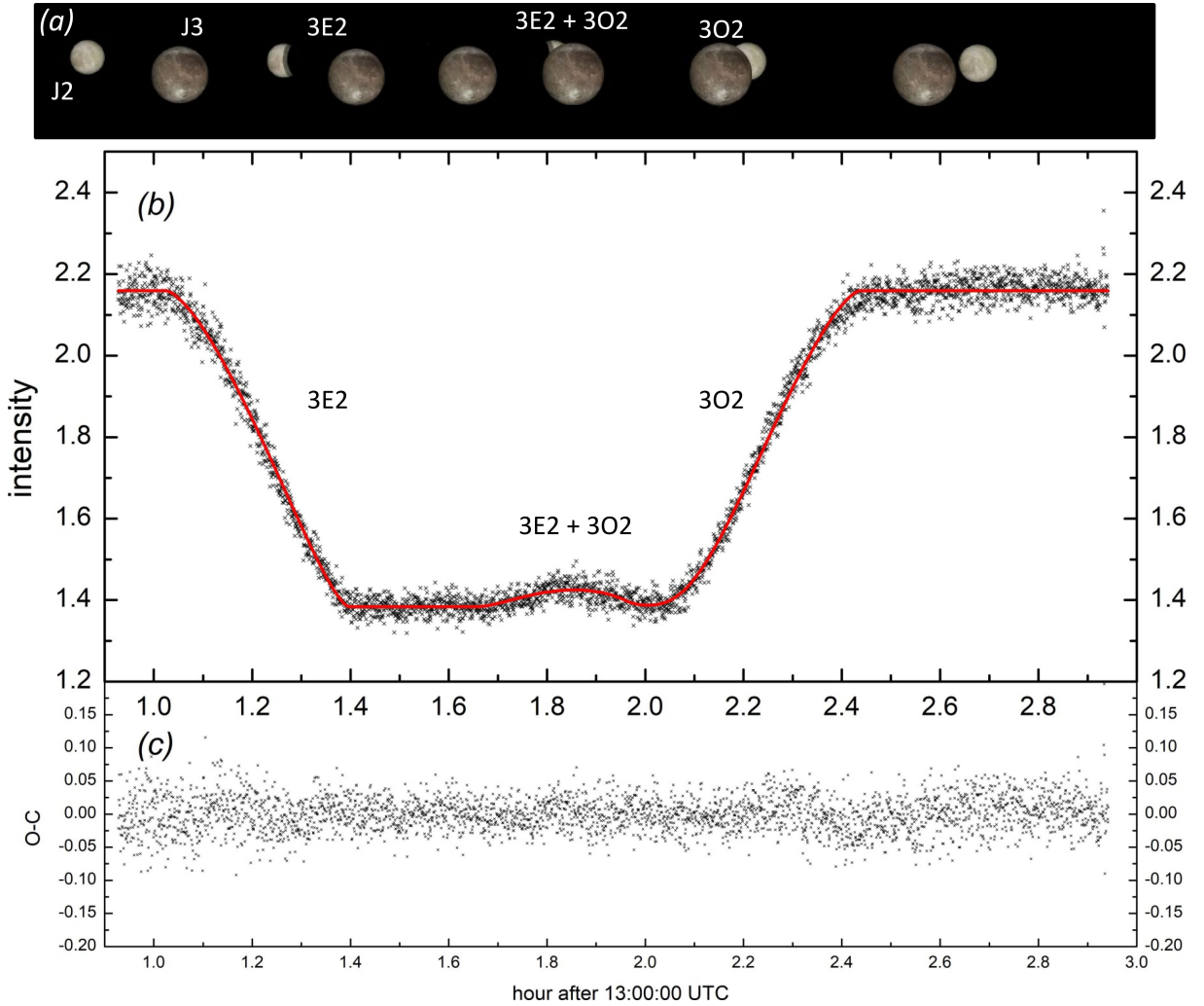


Figure 4: The 3E2 + 3O2 event on 22 August 2021. (a): sequential simulations created with WinJUPOS (<http://www.grischa-hahn.homepage.t-online.de/>); (b): observed data points and the fitted light curve in red; (c): O-C.

of sunlight over the penumbra, we opt to use a simple geometrical model in which the apparent radius of the eclipsing satellite r_e is used as the effective apparent radius of the penumbra. Using the formulae in Emelyanov (2003), r_e is $\sim 17\%$ larger than the apparent radius of umbra while r_e is $\sim 13\%$ smaller than apparent radius of penumbra. In view of the fact that a larger umbra would overestimate the shadow darkening, on the other hand, a smaller penumbra would underestimate the shadow darkening, we argue that our simplification is justifiable. Since the same satellite acted as the eclipsing and the occulting satellites in our case, r_e equals the apparent radius of the occulting satellite r_o . Specifically, obtained from NASA JPL's *Horizons System*,⁴ $r_e = r_o = 0.90535''$ and $r_p = 0.537''$ is the apparent radius of the passive satellite. k_{ep} is the area covered by the umbra. Similarly, k_{op} is the area covered by the occulting satellite. k is the overlapping area among the passive satellite, the active satellite and the umbra. For an ordinary ME, $k = 0$ and either k_{ep} or k_{op} is to be considered. Note that $[\pi r_p^2 - k_{ep}(t) - k_{op}(t) + k(t)]$ gives the uncovered area of the passive satellite when the passive satellite was eclipsed *AND* occulted simultaneously (see Fig. 5). $S = 1$ outside the QSME when all k 's are zero.

From the astrometric point of view as depicted in Fig. 6, the parameters used to describe the case include:

⁴<https://ssd.jpl.nasa.gov/horizons/app.html>.

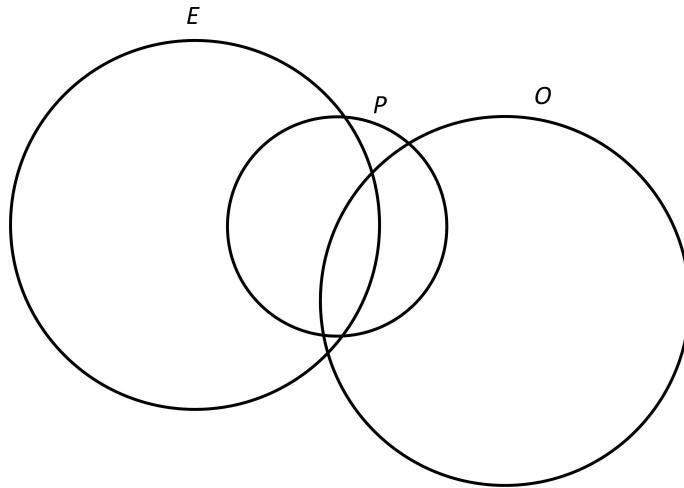


Figure 5: Relative positions of the occulting (O) and passive (P) satellites and the shadow (E) of the eclipsing satellite when the passive satellite was eclipsed *AND* occulted simultaneously.

- the impact parameter x_e , which is the closest distance between the centres of the circles P (the passive satellite) and E (the umbra of the eclipsing satellite);
- the impact parameter x_o , which is the closest distance between the centres of the circles P (the passive satellite) and O (the occulting satellite);
- the satellites' relative speeds v_o and v_e ; and
- the angle α between the eclipse and the occultation paths.

Differ from ordinary ME models, α is included because the eclipse and the occultation do not necessarily have to be along the same “path”. α_e and α_o are also defined as illustrated in Fig. 7.

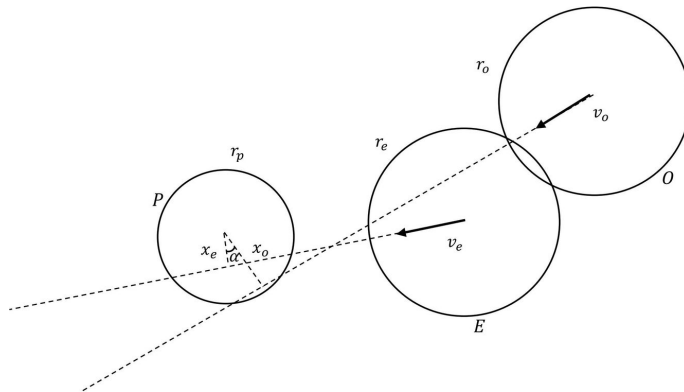


Figure 6: Geometry of the QSME model.

Here, to model the mutual eclipse and occultation simultaneously, the satellites' positions are projected onto the plane passing through the centres of both satellites and the plane is perpendicular to the beam directed to the satellites from the observer on Earth. For the mutual eclipse, this assumption differs from ordinary models where the plane is perpendicular to the beam directed to the satellites from the centre of the Sun (Emelyanov, 2020). We demonstrate in the phase angle analysis in Appendix E that the astrometric discrepancies originating from the mismatch of projection planes are much smaller than the overall error of each parameter (see Table 3).

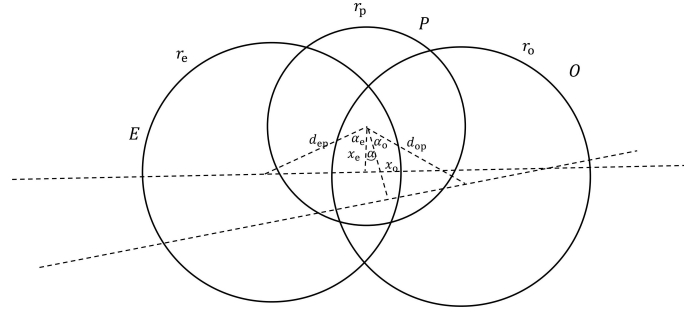


Figure 7: Same as Fig. 6 when the passive satellite was eclipsed AND occulted simultaneously.

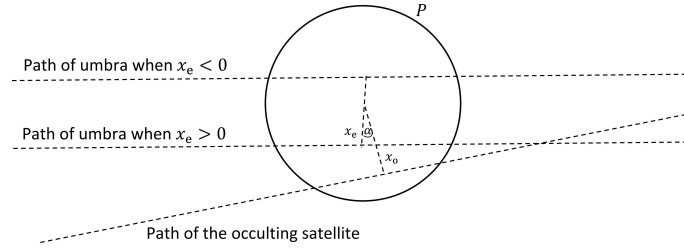


Figure 8: Signs of x_e and the path of the umbra relative to the path of the occulting satellite.

We also assume that the circles P , E and O are perfect, given that the satellites' phase angles are small during the event.

According to Assafin et al. (2009), we define $d^2 = x^2 + v^2 \cdot (t - t_{\text{central}})^2$, in which t_{central} is the central time of an individual event, i.e., when the eclipse or occultation is at its maximum. Then at any given time, the distances between the centres of the circles P , E and O can be obtained from the following three equations:

$$\begin{aligned} d_{op} &= \sqrt{x_o^2 + v_o^2(t - t_o)^2} , \\ d_{ep} &= \sqrt{x_e^2 + v_e^2(t - t_e)^2} \text{ and} \\ d_{eo} &= \sqrt{d_{ep}^2 + d_{op}^2 - 2d_{ep}d_{op} \cos \beta} , \end{aligned}$$

where the formulation of β depends on the sign of x_e . If $x_e > 0$, then $\beta = \alpha + \alpha_e + \alpha_o$. If $x_e < 0$, i.e., the path of the umbra is on the opposite side of the circle, then $\beta = \pi + \alpha + \alpha_e + \alpha_o$ or $\beta = \pi - (\alpha + \alpha_e + \alpha_o)$ depending on which one is smaller than π . See Fig. 8. In both cases, $\alpha_e = \tan^{-1} \left[\frac{v_e(t - t_e)}{x_e} \right]$ and $\alpha_o = \tan^{-1} \left[\frac{v_o(t_o - t)}{x_o} \right]$.

The geometric problem becomes expressing k 's in terms of r_p , r_o , r_e , d_{op} , d_{ep} and d_{eo} , and can partially be tackled by finding the "area of common overlap of three circles". This has been solved by considering multiple coordinate systems in Fewell (2006) (Appendix A). By geometry, we obtain

$$\begin{aligned} k_{op} &= (x''_{op} - d_{op}) \sqrt{r_p^2 - (x''_{op} - d_{op})^2} + r_p^2 \sin^{-1} \left(\frac{x''_{op} - d_{op}}{r_p} \right) \\ &\quad + r_p^2 \frac{\pi}{2} + r_o^2 \frac{\pi}{2} - x''_{op} \sqrt{r_o^2 - (x''_{op})^2} - r_o^2 \sin^{-1} \left(\frac{x''_{op}}{r_o} \right) , \end{aligned}$$

Table 2

O–C’s of satellite-satellite positional differences in milliarcseconds (mas).

Date	Event	Model	Theory, ephemerides	O-C (RA)	O-C (DEC)
22 August 2021	3E2	present study	Lainey et al. (2009); Fienga et al. (2020)	-25.9	30.3
22 August 2021	3O2	present study	Lainey et al. (2009); Fienga et al. (2020)	-6.2	17.9
29 January 1991	2O1	present study	Lainey et al. (2009); Fienga et al. (2020)	36.0	55.3
29 January 1991	2E1	present study	Lainey et al. (2009); Fienga et al. (2020)	0.5	0.5
29 January 1991	2O1	Vasundhara (1994)	Lieske (1977, 1987)	-61.9	-204.1
29 January 1991	2E1	Vasundhara (1994)	Lieske (1977, 1987)	26.1	87

$$k_{ep} = (x'_{ep} - d_{ep})\sqrt{r_p^2 - (x'_{ep} - d_{ep})^2} + r_p^2 \sin^{-1}\left(\frac{x'_{ep} - d_{ep}}{r_p}\right) \\ + r_p^2 \frac{\pi}{2} + r_e^2 \frac{\pi}{2} - x'_{ep} \sqrt{r_e^2 - (x'_{ep})^2} - r_e^2 \sin^{-1}\left(\frac{x'_{ep}}{r_e}\right)$$

and

$$k_{eo} = (x_{eo} - d_{eo})\sqrt{r_o^2 - (x_{eo} - d_{eo})^2} + r_o^2 \sin^{-1}\left(\frac{x_{eo} - d_{eo}}{r_o}\right) \\ + r_o^2 \frac{\pi}{2} + r_e^2 \frac{\pi}{2} - x_{eo} \sqrt{r_e^2 - x_{eo}^2} - r_e^2 \sin^{-1}\left(\frac{x_{eo}}{r_e}\right).$$

The details on formulating k_{op} , k_{ep} and k_{eo} are provided in Appendix B. The details on formulating k , which depends on the configurations of the circles P , E and O at a given instant, are provided in Appendix C.

The above formulations assume that both satellites have uniform albedos and there is no contribution of light reflected from Jupiter (“Jupiter-shine”, see Emelyanov et al. (2011) for the argument).

We fitted our observations against Eq. 1 by the Orthogonal Distance Regression (ODR) algorithm (Zwolak et al., 2007) provided in the data analysis software *OriginLab* 2022 Pro version.⁵ The fitting parameters are x_e , x_o , v_e , v_o , t_e , t_o , P_a/P_p , α and K . The next Section presents the fitting results.

5. Results

The fitted curve and the O-C residual plot are presented in Fig. 4(b) and (c) respectively. As seen from the figures, the fitted curve matches with the observations very well and the absolute values of the residuals are small and no obvious trend is detected.

We calculated the J3–J2 positional differences in right ascension (RA, α) and declination (DEC, δ), i.e., $\Delta\alpha \cos \delta$ and $\Delta\delta$ respectively, at the t_{central} from the fitted x and the position angle obtained from the Lainey et al. (2009)’s theory with the INPOP19a planetary ephemerides (Fienga et al., 2020) on *MULTI-SAT*.⁶ The corresponding O-C’s are presented in Table 2. The positional differences show a good agreement with the theory. Particularly, the sizes of our O-C’s are very similar to those of previous ME studies reported for the last four observation campaigns (PHEMU03, PHEMU09, PHEMU15 and PHEMU21, see Arlot and Emelyanov, 2019; Emelyanov et al., 2022). Notably, our occultation results have smaller discrepancies.

We derived the beginning time, ending time and flux drop ratio from the fitted model. Table 3 shows the fitted and derived parameters and the O-C residuals for the parameters predicted by *MULTI-SAT* in Table 1. In addition, the O-C’s of satellites’ relative speeds were compared with those computed from INPOP19a. Since the satellites’ phase angles during the QSME were very small ($0.680^\circ - 0.695^\circ$), the O-C of satellites’ albedos ratio was compared with those at 0° phase angle listed on the *MULTI-SAT*’s website⁷ ($P_{J3}/P_{J2} = 0.43/0.64 = 0.672$). The comparison takes

⁵<https://www.originlab.com/2022>.

⁶<http://nsdb.imcce.fr/multisat/nssreq5he.htm>.

⁷<http://nsdb.imcce.fr/multisat/parcohe.htm>.

Table 3

Results of the model fitted to the observations of the QSME event on 22 August 2021. O-C residuals refer to the predictions by *MULTI-SAT* (Table 1). See the text for remarks on the eclipse's O-C's.

Parameter	Description (unit)	Fitted value \pm standard error	O-C
3E2			
x_e	impact parameter (arcsec)	0.103 ± 0.119	0.078
v_e	relative speed at $t_{e,central}$ (arcsec hr ⁻¹)	2.855 ± 0.058	0.175
$t_{e,begin}$	beginning time (hour after 13:00)	1.018 ± 0.016	0.034
$t_{e,central}$	central time (hour after 13:00)	1.525 ± 0.011	0.012
$t_{e,end}$	ending time (hour after 13:00)	2.031 ± 0.016	-0.013
ΔI_e	flux drop ratio	0.639 ± 0.001	-0.014
3O2			
x_o	impact parameter (arcsec)	0.386 ± 0.004	-0.019
v_o	relative speed at $t_{o,central}$ (arcsec hr ⁻¹)	3.153 ± 0.026	0.012
$t_{o,begin}$	beginning time (hour after 13:00)	1.529 ± 0.005	-0.036
$t_{o,central}$	central time (hour after 13:00)	2.003 ± 0.002	-0.004
$t_{o,end}$	ending time (hour after 13:00)	2.477 ± 0.005	0.029
ΔI_o	flux drop ratio	0.641 ± 0.001	-0.017
QSME			
P_a/P_p	ratio of satellites' albedos	0.624 ± 0.001	-0.048
α	eclipse-occultation path separation angle (radian)	-0.210 ± 0.055	...
K	proportionality constant	2.161 ± 0.001	...

the ‘‘opposition surge’’, i.e. the surge in brightness when the object has a very small phase angle (Fujii et al., 2014; Buratti, 1995), into account. As noted in Sect. 4 and detailed in Appendix E, we computed the O-C of 3E2's parameters even though the projection planes of our model and those used in *MULTI-SAT*'s predictions were different. The fitting yields a negative x_e . We report the absolute value of x_e in Table 3 and compare the value with the prediction.

As a visual validation, we created an animated simulation based on the fitted parameters in <https://www.geogebra.org/calculator/rx6efjeu>.

Previous studies analysed multiple light curves obtained from different ordinary MEs and published the O-C's for each event. We compared our O-C values on the flux drop ratio (-2.1% and -2.6% for the mutual eclipse and occultation respectively) with the ranges of O-C of previous studies. The measured O-C's of flux drops reported in Peng and Noyelles (2007) ranged from -4% to 9% (excluding one observation with an O-C valued -45%). Similarly, the O-C's reported in Vienne et al. (2003) ranged from -26% to 10% . Zhang and X. L. Han (2019) even reported a O-C of mutual eclipse magnitude drop as large as -80% and a O-C of mutual occultation magnitude drop as large as 2100% .

We also compared our O-C values on the central time (43.2 and -14.4 s for the mutual eclipse and occultation respectively) with the ranges of O-C of previous studies. Based on the predictions from Lainey et al. (2009)'s theory, Dias-Oliveira et al. (2013) reported that the O-C of mutual eclipses ranged from -41.6 to 22 s while that of mutual occultations ranged from -10.9 to 19.2 s. Based on the computations of E3 ephemerides (Lieske, 1977, 1987), Vasundhara (1994) reported that the O-C of mutual eclipses ranged from -6.9 to 36.1 s while that of mutual occultations ranged from 18.0 to 37.5 s (excluding one observation with poor data quality).

In sum, we conclude that the absolute values of O-C in the present study are comparable to or even smaller than those of the previous studies in most of the cases. In other words, our simple geometric model is reasonably accurate with the high-quality data obtained in our observations.

5.1. Separate the light curve into an eclipse and an occultation counterparts

To validate the hypothesis that the observed QSME is a superposition of the eclipse and the occultation counterparts, we attempted to separate the QSME light curve into individual counterparts, based on the assumption that the eclipse and occultation light curves are symmetric before and after the corresponding central time ($t_{e,central}$ and $t_{o,central}$).

First, we reproduced the second half of the 3E2 light curve by mirroring the observations before the fitted $t_{e,central}$ (see Table 3). Second, we fitted the complete 3E2 light curve against the model presented in Fig. 4. The model was simplified to include the eclipse part only, i.e., setting $k_{op} = k = 0$ in Eq. 2. Similarly for the occultation, we reproduced

Table 4

Separation and fitting of the eclipse and the occultation counterparts of the QSME event on 22 August 2021. O-C residuals refer to the predictions by *MULTI-SAT* (Table 1). See Table 3 for the parameters' units.

Parameter	3E2 only		3O2 only		O-C
	Fitted value	\pm standard error	Fitted value	\pm standard error	
x_e	0.005	± 0.436	-0.020
v_e	2.880	± 0.010	0.200
ΔI_e	0.640	± 0.001	-0.012
x_o	0.401	± 0.022	-0.005
v_o	3.157	± 0.019	0.016
ΔI_o	0.639	± 0.008	-0.018
P_a/P_p	0.626	± 0.002	0.610	± 0.016	-0.046 & -0.062

the complete 3O2 light curves by mirroring the observations after the fitted $t_{o,central}$ (see Table 3) and conducted the fitting against the simplified occultation-only model, i.e., setting $k_{cp} = k = 0$ in Eq. 2. Fig. 9 shows the half-observed-half-reproduced light curves and their fitted curves. Table 4 tabulates the fitting results and O-C comparisons.

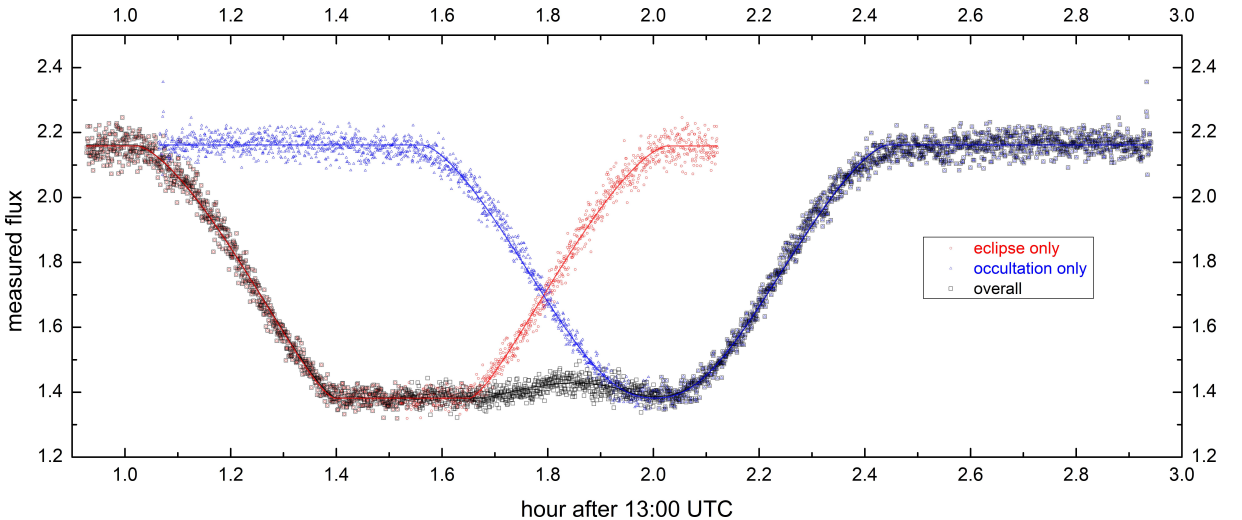


Figure 9: Separation of the eclipse and the occultation counterparts of the QSME event on 22 August 2021. The fitted light curves are overlaid on the data points. See the text for details.

As seen from Fig. 9 and the results in Table 4, the fittings are good and the absolute values of O-C's are very small in general. The separation of the QSME light curve has been successful.

Relatively large O-C discrepancies are only found on v_e from both the combined (6.5%, see Table 3) and the separated (8.1%, see Table 4) fittings. We attribute the large discrepancies to our model's incapability of including the satellites' acceleration. Future works are required to take the acceleration, although small, into consideration.

5.2. Fitting the 2O1 + 2E1 observation on 29 January 1991

As mentioned in Sect. 1 and simulated in Fig. 1(c), a QSME of 2O1 + 2E1 happened on 29 January 1991. The database of the Institut de Mécanique Céleste et de Calcul des Ephémérides (IMCCE)'s Natural Satellites Service archives several sets of photometric measurements of the event. We fitted the one with the best data quality taken from the Observatory at Calern in France (*dgrav2oe1.291* channel V dataset, converted to linear intensity) with the present model. The fitted asymmetric light curve and the O-C residual plot are presented in Fig. 10(a) and (b) respectively. Table 5 shows the fitted parameters and their errors. The fitting is very good and yields a negative x_e . We report the absolute value of x_e in Table 5 and compare the value with the prediction.

Similarly to our 2021 observations, we present the comparisons between theoretical J2–J1 positional differences and our calculations in Table 2. O-C's published by Vasundhara (1994) on the same event (but different observations)

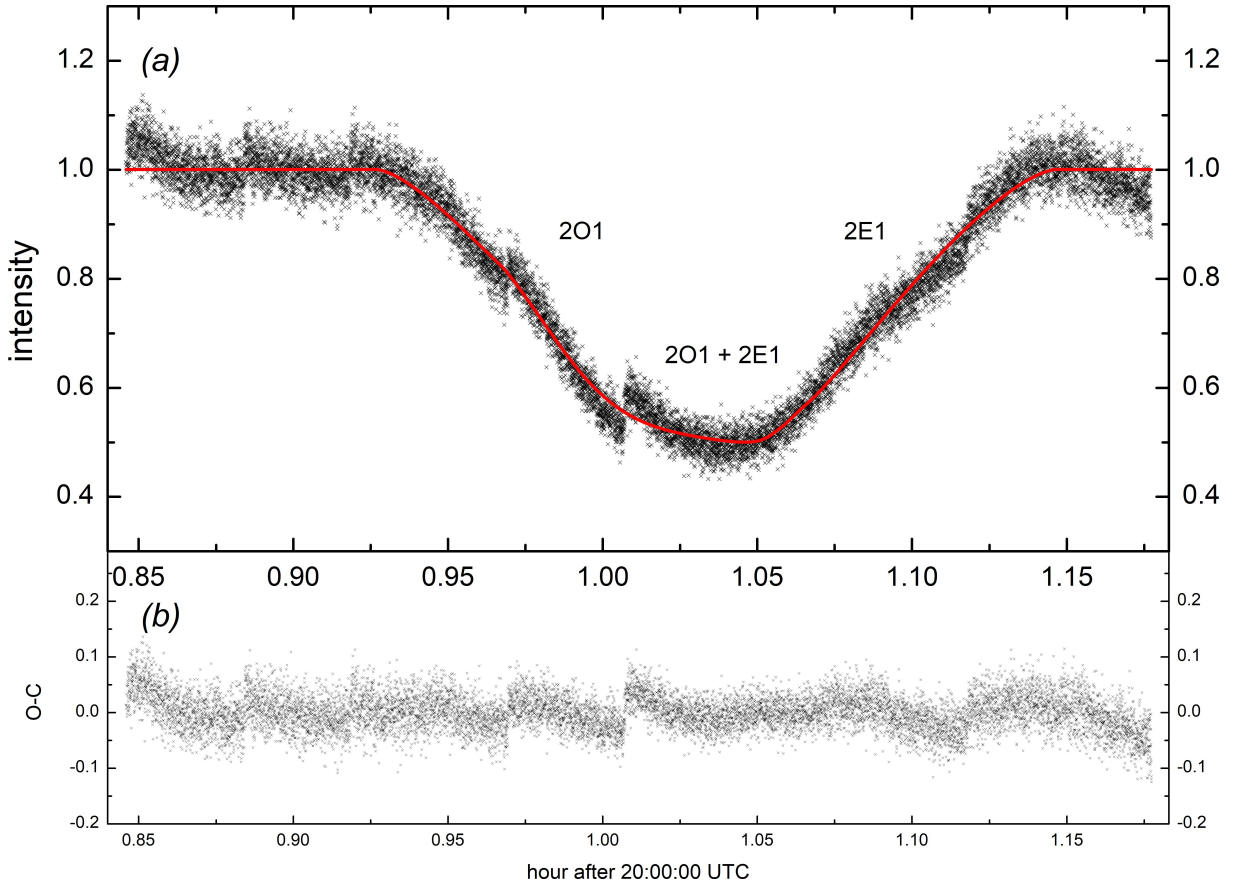


Figure 10: The 2O1 + 2E1 event on 29 January 1991. (a): observed data points (by others) and the fitted light curve in red; (b): O-C.

Table 5

Results of our model fitted to the observations of the QSME event by others on 29 January 1991.

Parameter	Description (unit)	Fitted value \pm standard error	O-C
2O1			
x_o	impact parameter (arcsec)	0.395 ± 0.021	0.068
v_o	relative speed at $t_{o,central}$ (arcsec hr $^{-1}$)	14.107 ± 0.096	1.621
$t_{o,central}$	central time (hour after 20:00)	0.999 ± 0.001	0.001
2E1			
x_e	impact parameter (arcsec)	0.080 ± 0.000	0.029
v_e	relative speed at $t_{e,central}$ (arcsec hr $^{-1}$)	12.150 ± 0.095	2.038
$t_{e,central}$	central time (hour after 20:00)	1.057 ± 0.001	0.011
QSME			
P_a/P_p	ratio of satellites' albedos	0.871 ± 0.015	-0.145
α	eclipse-occultation path separation angle (radian)	-0.505 ± 0.071	...
K	proportionality constant	1.000 ± 0.001	...

are appended for reference. Our method is not only applicable to the 1991 observations but also produces results that are closer to the theoretical values.

6. Conclusions & Discussions

Previous works focused primarily on separated MEs. Under specific rare orbital configurations when the same satellite is eclipsed and occulted quasi-simultaneously, a QSME occurs. Few researchers observed QSMEs and even fewer attempted to analyse their light curves. The present study fills the gap by observing a QSME on 22 August 2021, analysing the light curve and developing a model to obtain astrometric parameters.

Our study demonstrated that the QSME can be observed as easily as ordinary MEs. The QSME created an asymmetric and long (~ 1.5 h) light curve, which represents the superposition of an eclipse and an occultation counterparts. The light curve exhibited fine details such as the small amount of light escaped from the uncovered area of the near-total occulted satellite.

We also demonstrated that formulating the QSME by a simple geometric model is feasible. Despite the fact that high-order factors such as the effects of penumbra, satellites' surface albedo variations and Jupiter's halo had not been considered, the model successfully explained the entire QSME, with the absolute values of O-C's comparable to those of previous ME studies which adopted complicated models. Our simple model performs well as it describes two inter-correlated MEs (an eclipse *AND* an occultation) with improved sensitivity on the fitted parameters with respect to the observations on the QSME than those on individual MEs. Particularly in our case, the shape of the light curve during the period when the eclipse and the occultation occurred simultaneously places an additional constraint on the eclipse and the occultation parameters. In other words, obtaining more accurate results from QSME observations is possible even with a model that is not sophisticated. As demonstrated by fitting the 1991 QSME observations in Fig. 5.2, our model is generic and can be easily modified to apply to other cases. Future works include further testing our model with other observers' data (past or future).

Rough searches from the predictions of *MULTI-SAT* database⁸ and *Occult* software reveal that the Galilean satellites' orbital configurations do not favour any QSME during the next observing season in 2026–27. From *Occult*, the next QSME (2E3 + 2O3) occurring 04:42–04:56, 3 February 2033 seems to be the only QSME in the 2032–2033 observing season. Unfortunately, Jupiter will be very close ($\sim 39'$) to the Sun at that time because the Sun–Jupiter conjunction happens on 2 February, although daylight infrared ME observations have been shown possible (Arlot et al., 1990).

The next truly visible QSME (4E3 + 2O3 as simulated in Fig. 11) will occur on 6 January 2045. Indeed, 2045 is an unusual year in which at least four more QSMEs will happen in a multitude of different ways.⁹ QSMEs in 2045 collectively involve all Galilean satellites.

Given the rarity, our observation in 2021 remains unique in the short future.

The key to improving our knowledge of Solar System dynamics relies on accurate astrometric solutions reduced from many different ME observations covering extended periods (Emelyanov, 2020; Arlot and Emelyanov, 2019, 2009). Given that QSME observations serve the same purpose as demonstrated in the present work, we encourage professional and amateur observers to observe QSMEs in 2045 and beyond. In the meantime, we strongly encourage observers to release previous and future photometric data on QSMEs as much as possible to enrich the existing small database for examination and analysis.

Data Availability

The photometric measurements and astrometric results in the present study have been uploaded to the database of IMCCE's Natural Satellites Service.

Declaration of Competing Interest

None.

Acknowledgements

The authors thank Professor Ming-chung Chu for helpful discussions on the data analysis. G. Luk and G. Chung received support from the Department of Physics of The Chinese University of Hong Kong. E. Yuen received support

⁸<http://nsdb.imcce.fr/multisat/nsszph5he.htm>.

⁹2O3 + 2E3, 00:07–00:22, 6 February 2045; 2O1 + 2E1, 02:21–02:28, 7 February 2045; 3E2 + 3O2, 15:40–15:49, 8 February 2045; 2E1 + 2O1, 15:32–15:44, 10 February 2045. Occurrences are predicted by *Occult* software.

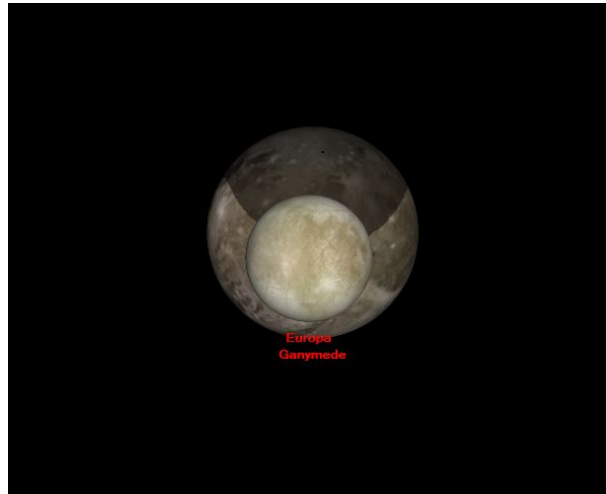


Figure 11: Next visible QSME (4E3 + 2O3) will occur 19:09–19:35, 6 January 2045. The shadow belongs to J4 instead of the occulting satellite J2. This event kick-starts a few more QSMEs in the same year. Simulations created with WinJUPOS (<http://www.grischa-hahn.homepage.t-online.de/>)

from the Department of Physics of The University of Hong Kong. We would also like to thank reviewers for taking the time and effort necessary to review the manuscript.

References

- Aksnes, K., 1974. Mutual phenomena of Jupiter's Galilean satellites, 1973-74. *Icarus* 21, 100–111. URL: <https://www.sciencedirect.com/science/article/abs/pii/0019103574900967>, doi:10.1016/0019-1035(74)90096-7.
- Aksnes, K., Franklin, F.A., 1976. Mutual phenomena of the Galilean satellites in 1973. III-Final results from 91 light curves. *Astron. J.* 81, 464–481. URL: <https://adsabs.harvard.edu/abs/1976AJ....81..464A>, doi:10.1086/111908.
- Aksnes, K., Franklin, F.A., 2001. Secular Acceleration of Io Derived from Mutual Satellite Events. *Astron. J.* 122, 2734–2739. URL: <https://iopscience.iop.org/article/10.1086/323708/meta>, doi:10.1086/323708.
- Arlot, J.E., Emelyanov, N., 2019. Natural satellites mutual phenomena observations: Achievements and future. *Planet. Space Sci.* 169, 70–77. URL: <https://www.sciencedirect.com/science/article/abs/pii/S0032063318301922>, doi:10.1016/j.pss.2019.02.004.
- Arlot, J.E., Emelyanov, N., 2020. The Campaign of Observation of the Mutual Occultations and Eclipses of the Galilean Satellites of Jupiter in 2021. *J. Occult. Astron.* 10, 3–10. URL: <https://adsabs.harvard.edu/abs/2020J0A...10d...3A>.
- Arlot, J.E., Emelyanov, N., Varfolomeev, M.I., Amossé, A., Arena, C., Assafin, M., Barbieri, L., Bolzoni, S., Bragas-Ribas, F., Camargo, J.I.B., Casarramona, F., Casas, R., Christou, A., Colas, F., Collard, A., Combe, S., Constantinescu, M., Dangl, G., Cat, P.D., Degenhardt, S., Delcroix, M., Dias-Oliveira, A., Dourneau, G., Douvris, A., Druon, C., Ellington, C.K., Estraviz, G., Farissier, P., Farmakopoulos, A., Garlitz, J., Gault, D., George, T., Gorda, S.Y., Grismore, J., Guo, D.F., Herald, D., Ida, M., Ishida, M., Ivanov, A.V., Klemt, B., Koshkin, N., Campion, J.F.L., Liakos, A., Liao, S.L., Li, S.N., Loader, B., Lopresti, C., Savio, E.L., Marchini, A., Marino, G., Masi, G., Massallé, A., Maulella, R., McFarland, J., Miyashita, K., Napoli, C., Noyelles, B., Pauwels, T., Pavlov, H., Peng, Q.Y., Perell, C., Priban, V., Prost, J., Razemon, S., Rousselle, J.P., Rovira, J., Ruisi, R., Ruocco, N., Salvaggio, F., Sbaruffatti, G., Shakun, L., Scheck, A., Sciuto, C., da Silva Neto, D.N., Sinyayeva, N., Sofia, A., Sonka, A., Talbot, J., Tang, Z.H., Tejfel, V.G., Thuillot, W., Tigani, K., Timerson, B., Tontodonati, E., Tsamis, V., Unwin, M., Venable, R., Vieira-Martins, R., Vilar, J., Vingerhoets, P., Watanabe, H., Yin, H.X., Yu, Y., Zambelli, R., 2014. The PHEMU09 catalogue and astrometric results of the observations of the mutual occultations and eclipses of the Galilean satellites of Jupiter made in 2009. *Astron. Astrophys.* 572, A120. URL: <https://www.aanda.org/articles/aa/abs/2014/12/aa23854-14/aa23854-14.html>, doi:10.1051/0004-6361/201423854.
- Arlot, J.E., Emelyanov, N.V., 2009. The NSDB natural satellites astrometric database. *Astron. Astrophys.* 503, 631–638. URL: https://www.aanda.org/articles/aa/full_html/2009/32/aa11645-09/aa11645-09.html, doi:10.1051/0004-6361/200911645.
- Arlot, J.E., Thuillot, W., et al., C.R., 2009. The PHEMU03 catalogue of observations of the mutual phenomena of the Galilean satellites of Jupiter. *Astron. Astrophys.* 493, 1171–1182. URL: <https://www.aanda.org/articles/aa/abs/2009/03/aa10420-08/aa10420-08.html>, doi:10.1051/0004-6361:200810420.
- Arlot, J.E., Thuillot, W., Sévre, F., Vu, D.T., Descamps, P., 1990. A new campaign of observation of the mutual events of the Galilean satellites in 1991. *Astron. Astrophys.* 236, L19. URL: <https://adsabs.harvard.edu/abs/1990A%26A...236L..19A>.
- Assafin, M., Vieira-Martins, R., Braga-Ribas, F., Camargo, J.I.B., da Silva Neto, D.N., Andrei, A.H., 2009. Observations and analysis of mutual events between the Uranus main satellites. *Astron. J.* 137, 4046. URL: <https://iopscience.iop.org/article/10.1088/0004-6256/137/4/4046/meta>, doi:10.1088/0004-6256/137/4/4046.
- Berthier, J., Descamps, P., Vachier, F., Normand, J., Maquet, L., Deleflie, F., Colasa, F., Klotz, A., Teng-Chuen-Yu, J.P., Peyrot, A., Braga-Ribas, F., Marchis, F., Leroy, A., Bouley, S., Dubos, G., Pollock, J., Pauwels, T., Vingerhoets, P., Farrell, A., Sada, P.V., Reddy, V., Archer, K.,

- H.Hamanowao, 2020. Physical characterization of double asteroid (617) Patroclus from 2007/2012 mutual events observations. *Icarus* 352, 113990. URL: <https://www.sciencedirect.com/science/article/abs/pii/S0019103520303560>, doi:10.1016/j.icarus.2020.113990.
- Buratti, B.J., 1995. Photometry and surface structure of the icy Galilean satellites. *J Geophys. Res.: Planets* 100, 19061–19066. URL: <https://agupubs.onlinelibrary.wiley.com/doi/abs/10.1029/95JE00146>, doi:10.1029/95JE00146.
- Descamps, P., Arlot, J.E., Thuillot, W., Colas, F., Vu, D.T., Bouchet, P., Hainaut, O., 1992. Observations of the volcanoes of Io, Loki and Pele, made in 1991 at the ESO during an occultation by Europa. *Icarus* 100, 235–244. URL: <https://www.sciencedirect.com/science/article/abs/pii/S0019103592900323?via%3Dihub>, doi:10.1016/0019-1035(92)90032-3.
- Descamps, P., Marchis, F., Pollock, J., Berthier, J., Birlan, M., Vachier, F., Colasa, F., 2008. 2007 Mutual events within the binary system of (22) Kalliope. *Planet. Space Sci.* 56, 1851–1856. URL: <https://www.sciencedirect.com/science/article/abs/pii/S003206330800189X>, doi:10.1016/j.pss.2008.02.037.
- Dias-Oliveira, A., Vieira-Martins, R., Assafin, M., Camargo, J.I.B., Braga-Ribas, F., da Silva Neto, D.N., Gaspar, H.S., dos Santos, P.M.P., Domingos, R.C., Boldrin, L.A.G., Izidoro, A., Carvalho, J.P.S., and J. Sampaio, R.S., Winter, O.C., 2013. Analysis of 25 mutual eclipses and occultations between the Galilean satellites observed from Brazil in 2009. *MNRAS* 432, 225–242. URL: <https://academic.oup.com/mnras/article/432/1/225/1117425>, doi:10.1093/mnras/stt447.
- Emelyanov, N., 2002. Mutual Occultations and Eclipses of Galilean Satellites of Jupiter in 2002–2003. *Sol. Syst. Res.* 36, 353–354. URL: <https://link.springer.com/article/10.1023/A:1019584724193>, doi:10.1023/A:1019584724193.
- Emelyanov, N., 2003. A Method for Reducing Photometric Observations of Mutual Occultations and Eclipses of Planetary Satellites. *Sol. Syst. Res.* 37, 314–325. URL: <https://link.springer.com/article/10.1023%2FA%3A1025034400005>, doi:10.1023/A:1025034400005.
- Emelyanov, N., 2020. The Dynamics of Natural Satellites of the Planets. Elsevier. URL: <https://www.sciencedirect.com/book/9780128227046/the-dynamics-of-natural-satellites-of-the-planets>, doi:10.1016/C2019-0-04631-6.
- Emelyanov, N., Arlot, J.E., 2020. Astrometric results PHEMU-1985 and PHEMU-1991. *Planet. Space Sci.* 187, 104946. URL: <https://www.sciencedirect.com/science/article/abs/pii/S0032063319304507>, doi:10.1016/j.pss.2020.104946.
- Emelyanov, N., Arlot, J.E., Anbazhagan, P., André, P., Bardecker, J., Canaud, G., Coliac, J.F., Cantalapedra, J.D.E., Ellington, C.K., Fernandez, J.M., Forbes, M., Gazeas, K., Gault, D., George, T., Gourdon, F., Herald, D., Huber, D., Iglesias-Marzoa, R., Izquierdo, J., Lloveras, R.J., Kerr, S., Lasala, A., Guen, P.L., Leroy, A., Lutz, M., Maley, P., Mannchen, T., Mari, J.M., Maury, A., Newman, J., Palafouta, S., Gallego, J.P., Roger, P., Roschli, D., Selvakumar, G., Serra, V., Stuart, P., Turchenko, M., Vasundhara, R., Velasco, E., 2022. The PHEMU21 catalogue and astrometric results of the observations of the mutual occultations and eclipses of the Galilean satellites of Jupiter made in 2021. *MNRAS* 516, 3685–3691. URL: <https://academic.oup.com/mnras/article/516/3/3685/6694266>, doi:10.1093/mnras/stac2538.
- Emelyanov, N.V., Andreev, M.V., Berezhoia, A.A., Bekhtevab, A.S., Velikodskiie, S.N.V.Y.I., Vereshchaginab, I.A., Gorshyanovb, D.L., Devyatkinb, A.V., Izmailovb, I.S., Ivanovb, A.V., Irmambetova, T.R., Kozlov, V.A., Karashevichb, S.V., Kurenyac, A.N., Naidenb, Y.V., Naumovb, K.N., Parakhinc, N.A., Raskhozhev, V.N., Sergeev, S.A.S.A.V., Sokovb, E.N., Khovrichv, M.Y., Khurtskayab, E.V., V., M.M.C.N., 2011. Astrometric results of observations at Russian observatories of mutual occultations and eclipses of Jupiter's Galilean satellites in 2009. *Sol. Syst. Res.* 45, 264–277. URL: <https://link.springer.com/article/10.1134/S0038094611010035>, doi:10.1134/S0038094611010035.
- Emelyanov, N.V., Arlot, J.E., 2008. The natural satellites ephemerides facility MULTI-SAT. *Astron. Astrophys.* 487, 759–765. URL: <https://www.aanda.org/articles/aa/abs/2008/32/aa09790-08/aa09790-08.html>, doi:10.1051/0004-6361:200809790.
- Fewell, M.P., 2006. Area of Common Overlap of Three Circles. Technical Report. Maritime Operations Division, Defence Science and Technology Organisation. URL: <https://citeseerx.ist.psu.edu/viewdoc/download?doi=10.1.1.989.1088&rep=rep1&type=pdf>. dSTO-TN-0722.
- Fienga, A., Avdellidou, C., Hanuš, J., 2020. Asteroid masses obtained with INPOP planetary ephemerides. *MNRAS* 492, 589–602. URL: <https://academic.oup.com/mnras/article/492/1/589/5658701>, doi:10.1093/mnras/stz3407.
- Fujii, Y., Kimura, J., Dohm, J., Ohtake, M., 2014. Geology and Photometric Variation of Solar System Bodies with Minor Atmospheres: Implications for Solid Exoplanets. *Astrobiology* 14, 753–768. URL: <https://www.liebertpub.com/doi/10.1089/ast.2014.1165>, doi:10.1089/ast.2014.1165.
- Goguen, J.D., Sinton, W.M., Matson, D.L., Howell, R.R., Dyck, H.M., Johnson, T.V., Brown, R.H., Veeder, G.J., Lane, A.L., Nelson, R.M., Laren, R.A.M., 1988. Io Hot Spots: Infrared Photometry of Satellite Occultations. *Icarus* 76, 465–484. URL: <https://www.sciencedirect.com/science/article/abs/pii/S0019103588900152>, doi:10.1016/0019-1035(88)90015-2.
- Lainey, V., Arlot, J.E., Karatekin, O., Hoolst, T.V., 2009. Strong tidal dissipation in Io and Jupiter from astrometric observations. *Nature* 459, 957–959. URL: <https://www.nature.com/articles/nature08108>, doi:10.1038/nature08108.
- Lainey, V., Arlot, J.E., Vienne, A., 2004a. New accurate ephemerides for the Galilean satellites of Jupiter II. Fitting the observations. *Astron. Astrophys.* 427, 371–376. URL: <https://www.aanda.org/articles/aa/abs/2004/43/aa1271/aa1271.html>, doi:10.1051/0004-6361:20041271.
- Lainey, V., Duriez, L., Vienne, A., 2004b. New accurate ephemerides for the Galilean satellites of Jupiter I. Numerical integration of elaborated equations of motion. *Astron. Astrophys.* 420, 1171–1183. URL: <https://www.aanda.org/articles/aa/abs/2004/24/aa0565/aa0565.html>, doi:10.1051/0004-6361:20034565.
- Lainey, V., Duriez, L., Vienne, A., 2006. Synthetic representation of the Galilean satellites' orbital motions from L1 ephemerides. *Astron. Astrophys.* 456, 783–788. URL: <https://www.aanda.org/articles/aa/abs/2006/35/aa4941-06/aa4941-06.html>, doi:10.1051/0004-6361:20064941.
- Lieske, J.H., 1977. Theory of motion of Jupiter's Galilean satellites. *Astron. Astrophys.* 56, 333–352. URL: <https://adsabs.harvard.edu/abs/1977A%26A...56...333L>.
- Lieske, J.H., 1987. Galilean satellite evolution: observational evidence for secular changes in mean motions. *Astron. Astrophys.* 176, 146–158. URL: <https://articles.adsabs.harvard.edu/abs/1987A%26A...176...146L>.

- Mallama, A., 1992. Astrometry of the Galilean satellites from mutual eclipses and occultations. *Icarus* 95, 309–318. URL: <https://www.sciencedirect.com/science/article/abs/pii/001910359290046A>, doi:10.1016/0019-1035(92)90046-A.
- Noyelles, B., Lainey, V., Vienne, A., 2004. Observation and reduction of mutual events in the solar system. *Proc. Int. Astron. Union IAUC196*, 271–278. URL: <https://www.cambridge.org/core/journals/proceedings-of-the-international-astronomical-union/article/observation-and-reduction-of-mutual-events-in-the-solar-system/D2A78519D5773CFFF6A7D531AD2BC829>.
- Noyelles, B., Vienne, A., Descamps, P., 2003. Astrometric reduction of lightcurves observed during the PHESAT95 campaign of Saturnian satellites. *Astron. Astrophys.* 401, 1159–1175. URL: <https://www.aanda.org/articles/aa/abs/2003/15/aa3319/aa3319.html>, doi:10.1051/0004-6361:20030214.
- Pauwels, T., Vingerhoets, P., Cuyper, J., 2005. Photometric observations of the mutual phenomena of the Galilean Satellites of Jupiter in 1997 and 2003 at the Royal Observatory of Belgium. *Astron. Astrophys.* 437, 705–710. URL: <https://www.aanda.org/articles/aa/abs/2005/26/aa1580-04/aa1580-04.html>, doi:10.1051/0004-6361:20041580.
- Peng, Q.Y., Noyelles, B., 2007. Eclipses and Occultations of Galilean Satellites Observed at Yunnan Observatory in 2003. *Chin. J. Astron. Astrophys.* 7, 317–324. URL: <https://iopscience.iop.org/article/10.1088/1009-9271/7/2/16>, doi:10.1088/1009-9271/7/2/16.
- Price, F.W., 2000. *The Planet Observer's Handbook*. Cambridge University Press. URL: <https://www.cambridge.org/core/books/planet-observers-handbook/F00D8EAC3290F76FC9CD71761E3F6F9F>, doi:10.1017/CB09780511600241.
- Pun, C.S.J., So, C.W., Leung, W.Y., Wong, C.F., 2013. Contributions of artificial lighting sources on light pollution in Hong Kong measured through a night sky brightness monitoring network. *J. Quant. Spectrosc. Radiat. Transf.* 139, 90–108. URL: <http://www.sciencedirect.com/science/article/pii/S0022407313004950>, doi:10.1016/j.jqsrt.2013.12.014.
- Saquet, E., Emelyanov, N., Colas, F., Robert, J.E.A.V., Christophe, B., Dechambre, O., 2016. Eclipses of the inner satellites of Jupiter observed in 2015. *Astron. Astrophys.* 591, A42. URL: <https://www.aanda.org/articles/aa/abs/2016/07/aa28246-16/aa28246-16.html>, doi:10.1051/0004-6361/201628246.
- Saquet, E., Emelyanov, N., Robert, V., Arlot, J.E., Anbazhagan, P., Baillie, K., Bardecker, J., Bereznoy, A.A., Bretton, M., Campos, F., Capannoli, L., Carry, B., Castet, M., Chernikov, Y.C.M.M., Christou, A., Colas, F., Coliac, J.F., Dangl, G., Dechambre, O., Delcroix, M., Dias-Oliveira, A., Drillaud, C., Duchemin, Y., Dunford, R., Dupouy, P., Ellington, C., Fabre, P., Filipov, V.A., Finnegan, J., Foglia, S., Font, D., Gaillard, B., Galli, G., Garlitz, J., Gasmi, A., Gaspar, H.S., Gault, D., Gazeas, K., George, T., Gorda, S.Y., Gorshonov, D.L., Gualdoni, C., Guhl, K., Halir, K., Hanna, W., Henry, X., Herald, D., Houdin, G., Ito, Y., Izmailov, I.S., Jacobsen, J., Jones, A., Kamoun, S., Kardasis, E., Karimov, A.M., Khovritchev, M.Y., Kulikova, A.M., Laborde, J., Lainey, Lavayssiere, M., Guen, P.L., Leroy, A., Loader, B., Lopez, O.C., Lyashenko, A.Y., Lyssenko, P.G., Machado, D.I., Maigurova, N., Manek, J., Marchini, A., Midavaine, T., Montier, J., Morgado, B.E., Naumov, K.N., Nedelcu, A., Newman, J., Ohlert, J.M., Oksanen, A., Pavlov, H., Petrescu, E., Pomazan, A., Popescu, M., Pratt, A., Raskhozhev, V.N., Resch, J.M., Robilliard, D., Roschina, E., Rothenberg, E., Rottenborn, M., Rusov, S.A., Saby, F., Saya, L.F., Selvakumar, G., Signoret, F., Slesarenko, V.Y., Sokov, E.N., Soldateschi, J., Soulie, A., Talbot, J., V.G.Tejfel, Thuillot, W., Timerson, B., Toma, R., Torsellini, S., Trabuco, L., Traverse, P., Tsamis, V., Unwin, M., Abbeel, F.V.D., Vandenbruaene, H., Vasundhara, R., Velikodsky, Y.I., Vienne, A., Vilar, J., Vugnon, J.M., Wuensche, N., Zeleny, P., 2018. The PHEMU15 catalogue and astrometric results of the Jupiter's Galilean satellite mutual occultation and eclipse observations made in 2014-2015. *MNRAS* 474, 4730–4739. URL: <https://academic.oup.com/mnras/article/474/4/4730/4644838>, doi:10.1093/mnras/stx2957.
- So, C.W., 2014. Observational studies of contributions of artificial and natural light factors to the night sky brightness measured through a monitoring network in Hong Kong. Ph.D. thesis. The University of Hong Kong. URL: <https://hub.hku.hk/handle/10722/206449>, doi:10.5353/th_b5317025.
- So, C.W., Leung, W.M.R., 2019. Light Pollution Monitoring at iObservatory and Astropark - Insights on Dark Sky Conservation in Hong Kong. *Hong Kong Museum Journal* 2, 74. URL: https://www.museums.gov.hk/documents/10347444/10348397/HKMuseumJournal_vol.2.pdf.
- Vasundhara, R., 1994. Mutual phenomena of the Galilean satellites: an analysis of the 1991 observations from VBO. *Astron. Astrophys.* 281, 565–575. URL: <https://adsabs.harvard.edu/abs/1994A%26A...281..565V>.
- Vasundhara, R., Selvakumar, G., Anbazhagan, P., 2017. Analysis of mutual events of Galilean satellites observed from VBO during 2014-2015. *MNRAS* 468, 501–508. URL: <https://academic.oup.com/mnras/article/468/1/501/3038264>, doi:10.1093/mnras/stx437.
- Vienne, A., 2008. Dynamical objectives of observation of mutual events. *Planet. Space Sci.* 56, 1797–1803. URL: https://www.sciencedirect.com/science/article/pii/S0032063308001785?casa_token=eJ0kVGLYEtcAAAAA:mXIwImlmPz1GJ0vfvSvf-CiCvc6rbG4aGMC0ZfTWM3gx5oj08fxvPs7DKLstgv1UcS2Xbrt5bV, doi:10.1016/j.pss.2008.02.036.
- Vienne, A., Noyelles, B., Amossé, A., 2003. Observation of 13 mutual events of Jovian satellites performed at Lille Observatory. *Astron. Astrophys.* 410, 343–347. URL: <https://www.aanda.org/articles/aa/abs/2003/40/aa4055/aa4055.html>, doi:10.1051/0004-6361:20031284.
- Zhang, X.L., X. L. Han, J.E.A., 2019. Mutual events between Galilean satellites observed with SARA 0.9 m and 0.6 m telescopes during 2014-2015. *MNRAS* 483, 4518–4524. URL: <https://academic.oup.com/mnras/article/483/4/4518/5173093?login=true>, doi:10.1093/mnras/sty3030.
- Zwolak, J.W., Boggs, P.T., Watson, L.T., 2007. Algorithm 869: ODRPACK95: a weighted orthogonal distance regression code with bound constraints. *ACM Trans. Math. Softw.* 33, 27. URL: <https://dl.acm.org/doi/abs/10.1145/1268776.1268782>, doi:10.1145/1268776.1268782.

Appendix A: Coordinate Systems

The coordinate systems follow Fewell (2006). As illustrated in Fig. 12, the origin of coordinates is placed at the centre of the circle E and the x -axis passes through the centre of the circle O . The direction of the y -axis is chosen so that the y -coordinate of the centre of the circle P is positive.

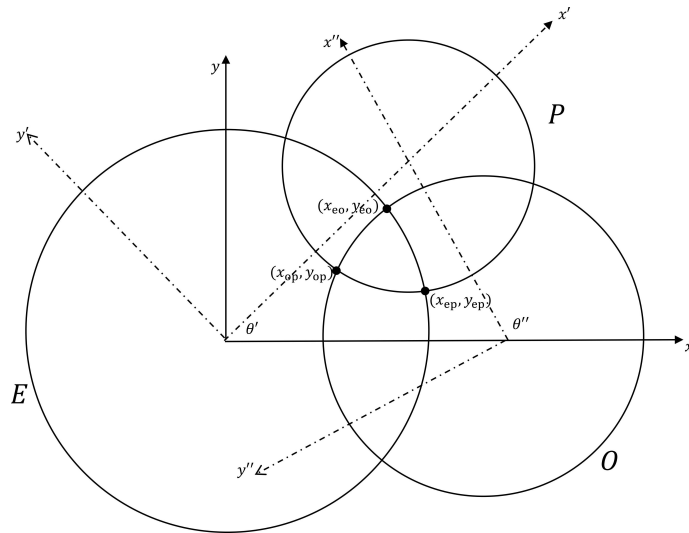


Figure 12: Coordinate systems for finding the area of common overlap of three circles.

The (x, y) system is appropriate for analysing the intersections of the circles E and O . To describe the third circle, for convenience, two other coordinate systems are used. They are labelled as (x', y') and (x'', y'') and obtained by rotating and translating the (x, y) coordinates:

- The origin of the (x', y') system locates at the centre of the circle E and the x' axis passes through the centre of the circle P .
- The origin of the (x'', y'') system locates at the centre of the circle O and the x'' axis passes through the centre of the circle P .

Fig. 12 also shows the angles θ' and θ'' between the x -axis and the respective abscissas of the two additional systems.

Before finding k_{op} , k_{ep} and k , let's find the three intersections among circles, namely (x_{eo}, y_{eo}) , (x_{ep}, y_{ep}) and (x_{op}, y_{op}) . The first set is:

$$x_{eo} = \frac{r_e^2 - r_o^2 + d_{eo}^2}{2d_{eo}} \quad \text{and}$$

$$y_{eo} = \frac{1}{2d_{eo}} \sqrt{2d_{eo}^2(r_e^2 + r_o^2) - (r_e^2 - r_o^2)^2 - d_{eo}^4} .$$

To find (x_{ep}, y_{ep}) , we need to find θ' using the cosine formula and (x'_{ep}, y'_{ep}) , which is the coordinate of the point in (x', y') . Similarly, to find (x_{op}, y_{op}) , we need to find θ'' using the cosine formula and (x''_{op}, y''_{op}) , which is the coordinate of the point in (x'', y'') . Specifically, related equations are:

$$\begin{aligned}
 \cos \theta' &= \frac{d_{eo}^2 + d_{ep}^2 - d_{op}^2}{2d_{eo}d_{ep}}, \\
 \sin \theta' &= \sqrt{1 - \cos^2 \theta'}, \\
 x'_{ep} &= \frac{r_e^2 - r_p^2 + d_{ep}^2}{2d_{ep}}, \\
 y'_{ep} &= -\frac{1}{2d_{ep}} \sqrt{2d_{ep}^2(r_e^2 + r_p^2) - (r_e^2 - r_p^2)^2 - d_{ep}^4}, \\
 \cos \theta'' &= -\frac{d_{eo}^2 + d_{op}^2 - d_{ep}^2}{2d_{eo}d_{op}}, \\
 \sin \theta'' &= \sqrt{1 - \cos^2 \theta''}, \\
 x''_{op} &= \frac{r_o^2 - r_p^2 + d_{op}^2}{2d_{op}} \text{ and} \\
 y''_{op} &= \frac{1}{2d_{op}} \sqrt{2d_{op}^2(r_o^2 + r_p^2) - (r_o^2 - r_p^2)^2 - d_{op}^4}.
 \end{aligned}$$

Now we can transform the point (x'_{ep}, y'_{ep}) and (x''_{op}, y''_{op}) back to the system (x, y) , i.e.,

$$\begin{aligned}
 x_{ep} &= x'_{ep} \cos \theta' - y'_{ep} \sin \theta', \\
 y_{ep} &= x'_{ep} \sin \theta' + y'_{ep} \cos \theta', \\
 x_{op} &= x''_{op} \cos \theta'' - y''_{op} \sin \theta'' + d_{eo} \text{ and} \\
 y_{op} &= x''_{op} \sin \theta'' + y''_{op} \cos \theta''.
 \end{aligned}$$

Appendix B: Formulating $k_{op}(t)$, $k_{ep}(t)$ and $k_{eo}(t)$

$k_{op}(t)$ can be found by integration in the coordinate system (x'', y'') (Fig. 13). Note that for $d_{op} > r_p + r_o$, $k_{op}(t) = 0$ since satellites do not overlap with each other. $k_{op}(t) = 1$ for the case that the passive satellite is completely occulted, i.e., $d_{op} < r_o - r_p$.

$$\begin{aligned}
 k_{op}(t) &= 2 \int_{d_{op}-r_p}^{x''_{op}} \sqrt{r_p^2 - (x - d_{op})^2} dx + 2 \int_{x''_{op}}^{r_o} \sqrt{r_o^2 - x^2} dx \\
 &= 2 \int_{-r_p}^{x''_{op}-d_{op}} \sqrt{r_p^2 - u^2} du + 2 \int_{x''_{op}}^{r_o} \sqrt{r_o^2 - x^2} dx \\
 &= \left[u \sqrt{r_p^2 - u^2} + r_p^2 \sin^{-1} \left(\frac{u}{r_p} \right) \right]_{-r_p}^{x''_{op}-d_{op}} \\
 &\quad + \left[x \sqrt{r_o^2 - x^2} + r_o^2 \sin^{-1} \left(\frac{x}{r_o} \right) \right]_{x''_{op}}^{r_o} \\
 &= (x''_{op} - d_{op}) \sqrt{r_p^2 - (x''_{op} - d_{op})^2} + r_p^2 \sin^{-1} \left(\frac{x''_{op} - d_{op}}{r_p} \right) \\
 &\quad + r_p^2 \frac{\pi}{2} + r_o^2 \frac{\pi}{2} - x''_{op} \sqrt{r_o^2 - (x''_{op})^2} - r_o^2 \sin^{-1} \left(\frac{x''_{op}}{r_o} \right).
 \end{aligned}$$

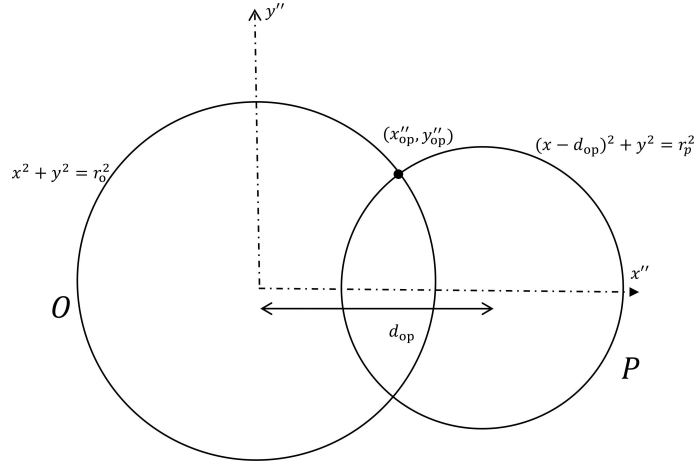


Figure 13: (x'', y'') coordinate system when finding $k_{op}(t)$.

Table 6

Graphical representations for finding $k(t)$.

$d_{eo} > r_o + r_p$	$d_{eo} < r_o - r_p $

Similarly, changing d_{op} , r_o , x''_{op} in $k_{op}(t)$ to d_{ep} , r_e , x'_{ep} respectively will provide $k_{ep}(t)$:

$$k_{ep}(t) = (x'_{ep} - d_{ep})\sqrt{r_p^2 - (x'_{ep} - d_{ep})^2} + r_p^2 \sin^{-1}\left(\frac{x'_{ep} - d_{ep}}{r_p}\right) \\ + r_p^2 \frac{\pi}{2} + r_e^2 \frac{\pi}{2} - x'_{ep}\sqrt{r_e^2 - (x'_{ep})^2} - r_e^2 \sin^{-1}\left(\frac{x'_{ep}}{r_e}\right).$$

Define k_{eo} as the overlapping area of the active satellite and the umbra divided by the passive satellite circle area. Similar to $k_{ep}(t)$ and $k_{op}(t)$, changing d_{ep} , r_p , x'_{ep} in k_{ep} to d_{eo} , r_o , x_{eo} respectively will provide $k_{eo}(t)$:

$$k_{eo}(t) = (x_{eo} - d_{eo})\sqrt{r_o^2 - (x_{eo} - d_{eo})^2} + r_o^2 \sin^{-1}\left(\frac{x_{eo} - d_{eo}}{r_o}\right) \\ + r_o^2 \frac{\pi}{2} + r_e^2 \frac{\pi}{2} - x_{eo}\sqrt{r_e^2 - x_{eo}^2} - r_e^2 \sin^{-1}\left(\frac{x_{eo}}{r_e}\right).$$

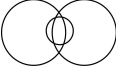
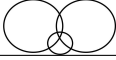
Appendix C: Formulating $k(t)$

$k(t)$ is the overlapping area of the passive satellite, the active satellite and the umbra at time t . Since $k(t)$ depends on the orientations of three circles, $k(t)$ is separated into different cases by considering the circle overlapping.

First, if any two circles do not intercept with each other, $k(t)$ can be found easily. For example, if the circles O and P do not intercept with each other, either $d_{eo} > r_o + r_p$ or $d_{eo} < |r_o - r_p|$ (see Table 6). In the former case, $k(t) = 0$. In the latter case, $k(t)$ equals to the overlapping area between the circle E and the smaller one among the circles O and P . Then, the configuration of three circles can be divided into different cases by three statements.

Table 7

Cases of $k(t)$ and configurations of the circles O , E and P .

Case	Configuration	$k(t) =$
IIO IOI OII		$k_{eo} + k_{op} - \pi r_o^2$ $k_{eo} + k_{ep} - \pi r_e^2$ $k_{op} + k_{ep} - \pi r_p^2$
IOO OIO OOI		k_{eo} k_{op} k_{ep}
OOO		0
Circular triangle		A_{CT}

1. The interceptions between the circles O and E are both inside (I) or both outside (O) the circle P .
2. The interceptions between the circles O and P are both inside or both outside the circle E .
3. The interceptions between the circles E and P are both inside or both outside the circle O .

For example, the case IOI means that the circles O and E both intercept inside the circle P , the circles O and P both intercept outside the circle E , while the circles E and P both intercept inside the circle O . Note that the case III does not exist.

$k(t)$ of all cases can be determined by considering four points, (x_{eo}, y_{eo}) , $(x_{eo}, -y_{eo})$, (x_{op}, y_{op}) , $(x_{ep}, -y_{ep})$ and their distances from the center of the circles. See Table 7 for a summary.

An additional case is that the interceptions are one inside and one outside of the third circle of all three circles. In that case, a circular triangle formed. So, to determine the circular triangle (A_{CT}) case, both interceptions between E and O are checked, which have the coordinates (x_{eo}, y_{eo}) and $(x_{eo}, -y_{eo})$. Appendix D introduces the calculation of A_{CT} .

Appendix D: Formulating A_{CT}

To find A_{CT} mentioned near the end of Appendix C, we need to find the lengths of the chords c_e , c_o and c_p as illustrated in Fig. 14 first:

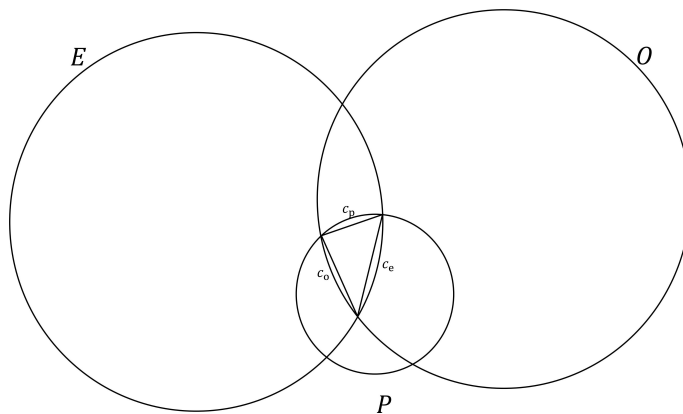


Figure 14: Circular triangle and the triangle area formed by three chords and three segments.

$$\begin{aligned}
 c_e &= \sqrt{(x_{ep} - x_{eo})^2 + (y_{ep} - y_{eo})^2} , \\
 c_o &= \sqrt{(x_{op} - x_{eo})^2 + (y_{op} - y_{eo})^2} \text{ and} \\
 c_p &= \sqrt{(x_{op} - x_{ep})^2 + (y_{op} - y_{ep})^2} .
 \end{aligned}$$

Then A_{CT} is given by the area of the triangle formed by three chords and three segments:

$$\begin{aligned}
 A_{CT} &= \frac{1}{4} \sqrt{(c_e + c_o + c_p)(c_e + c_o - c_p)(c_e + c_p - c_o)(c_o + c_p - c_e)} \\
 &\quad + \left(r_o^2 \sin^{-1} \frac{c_o}{2r_o} - \frac{c_o}{4} \sqrt{4r_o^2 - c_o^2} \right) \\
 &\quad + \left(r_e^2 \sin^{-1} \frac{c_e}{2r_e} - \frac{c_e}{4} \sqrt{4r_e^2 - c_e^2} \right) \\
 &\quad + \left(r_p^2 \sin^{-1} \frac{c_p}{2r_p} - \frac{c_p}{4} \sqrt{4r_p^2 - c_p^2} \right) .
 \end{aligned}$$

However, if more than half of the circle P is included in the circular triangle, i.e., the inequality

$$d_{ep} \sin \theta' < y_{ep} + \frac{y_{op} - y_{ep}}{x_{op} - x_{ep}} (d_{ep} \cos \theta' - x_{ep})$$

is true, then the last term of A_{CT} becomes $r_p^2 \left(\pi - \sin^{-1} \frac{c_p}{2r_p} \right) + \frac{c_p}{4} \sqrt{4r_p^2 - c_p^2}$.

Appendix E: Astrometric discrepancies originating from the projection planes mismatch

Previous studies had two different choices of coordinate projection planes to describe mutual eclipses and mutual occultations separately. *MULTI-SAT* predicts the satellite's longitude relative to the projection of the vector of the *Sun* on the equator of the planet (planetocentric planet-equatorial coordinate plane) for mutual eclipses. On the other hand, *MULTI-SAT* predicts the satellite's longitude relative to the projection of the vector of the *Earth* on the equator of the planet (synodic planetocentric coordinate plane) for mutual occultations (Emelyanov, 2020). The origin is placed at the eclipsed or occulted satellite.

While the above choices of coordinate planes are justified for individual QEs, we have to choose one of them if QSME is considered. Our model in Sect. 4 adopted the synodic coordinate plane in which the projection vector points from the observer on the Earth to the satellites. Since our choice favours mutual occultations, one may expect certain astrometric discrepancies when describing mutual eclipses. The discrepancies can be significant if the satellite's phase angle, i.e., the angle between coordinate planes, is larger (See Fig. 15).

From NASA JPL's *Horizons System*¹⁰, the phase angle during the QSME ranged from 0.680° to 0.695°. To estimate the size of the discrepancies, let us consider the x coordinates of the satellite's locus on both planes. From Fig. 16, the locus of J3 on the synodic coordinate plane is given by

$$\begin{cases} x_E = v_e(t - t_e) \sin \phi + x_e \cos \phi \\ y = -v_e(t - t_e) \cos \phi + x_e \sin \phi \end{cases} . \quad (3)$$

for an unknown value of ϕ in the (y, x_E) coordinate.

On the planet-equatorial coordinate plane (y, x_S) , since $x_E \cos \theta = x_S$, the locus is given by

$$\begin{cases} x_E = v_e(t - t_e) \sin \phi \cos \theta + x_e \cos \theta \cos \phi \\ y = -v_e(t - t_e) \cos \phi + x_e \sin \phi \end{cases} . \quad (4)$$

¹⁰<https://ssd.jpl.nasa.gov/horizons/app.html>

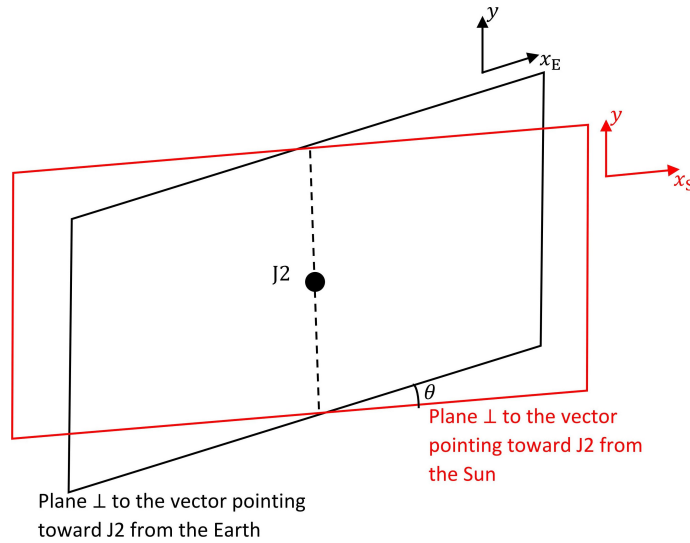


Figure 15: Two different choices of coordinate projection planes to describe mutual eclipses and mutual occultations.

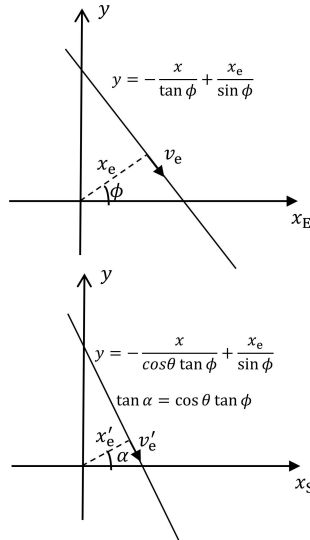


Figure 16: Coordinates of the satellite's locus on different coordinate projection planes.

To find x'_e , we use the fact that there are two ways to calculate the area of the right angle triangle,

$$\frac{1}{2} x'_e \sqrt{\left(\frac{x_e}{\sin \phi}\right)^2 + \left(\frac{x_e \cos \theta}{\cos \phi}\right)^2} = \frac{1}{2} \left| \frac{x_e}{\sin \phi} \right| \left| \frac{x_e \cos \theta}{\cos \phi} \right|, \quad (5)$$

$$x'_e = \frac{|\cos \theta|}{\sqrt{\sin^2 \phi \cos^2 \theta + \cos^2 \phi}} x_e. \quad (6)$$

The maximum change in x_e occurred when $\phi = 0$ or $\phi = \pi$. In these cases, $x'_e = x_e \cos \theta$.

To find v'_e ,

$$v'_e = \sqrt{(x'_E)^2 + (y')^2} = v_e \sqrt{\sin^2 \phi \cos^2 \theta + \cos^2 \phi}. \quad (7)$$

So the maximum change in v_e occurred when $\phi = \pi/2$ or $\phi = 3\pi/2$. In these cases, $v'_e = v_e \cos \theta$.

To find t'_e ,

$$x'_e \cos \alpha = v_e(t'_e - t_e) \sin \phi \cos \theta + x_e \cos \theta \cos \phi , \quad (8)$$

$$\frac{\cos \theta}{\sqrt{\sin^2 \phi \cos^2 \theta + \cos^2 \phi}} \cos \alpha = v_e(t'_e - t_e) \sin \phi \cos \theta + x_e \cos \theta \cos \phi . \quad (9)$$

Since $|\cos \alpha| = 1/\sqrt{\tan^2 \alpha + 1} = 1/\sqrt{\cos^2 \theta \tan^2 \phi + 1}$,

$$|t'_e - t_e| = \frac{x_e}{v_e} \left| \frac{\cos \phi \sin \phi \sin^2 \theta}{\sin^2 \phi \cos^2 \theta + \cos^2 \phi} \right| . \quad (10)$$

Plugging in our fitted values from Table 3, the astrometric discrepancies on x_e (in arcsec), v_e (in arcsec hr⁻¹) and t_e (in hr) due to the projection planes mismatch are limited to $(1 - \cos 0.695^\circ) \times x_e = 7.6 \times 10^{-6}$, $(1 - \cos 0.695^\circ) \times v_e = 2.1 \times 10^{-4}$ and $0.00614 \times x_e/v_e = 2.2 \times 10^{-4}$ respectively. They are at least one order of magnitude smaller than the parameter errors. To conclude, in view of the smallness of the phase angle, we can safely ignore the astrometric discrepancies and compute their O-Cs directly.